

Toroidal modeling of penetration of the resonant magnetic perturbation field

Yueqiang Liu¹, A. Kirk¹, and Y. Sun²

¹*Euratom/CCFE Fusion Association, Culham Science Centre, Abingdon, OX14 3DB, UK*

²*Institute of Plasma Physics, Chinese Academy of Sciences, PO Box 1126, Hefei 230031, China*

E-mail contact of the main author: yueqiang.liu@ccfe.ac.uk

abstract. A toroidal, quasi-linear model is proposed to study the penetration dynamics of the resonant magnetic perturbation (RMP) field into the plasma. The model couples the linear, fluid plasma response to a toroidal momentum balance equation, which includes torques induced by both fluid electromagnetic force and by (kinetic) neoclassical toroidal viscous force. The numerical results for a test toroidal equilibrium quantify the effects of various physical parameters on the field penetration and on the plasma rotation braking. The neoclassical toroidal viscous torque plays a dominant role in certain region of the plasma, for the RMP penetration problem considered in this work.

1 Introduction

It is expected that large scale, low frequency type-I edge localized modes (ELMs) may not be tolerable for the plasma facing components in ITER, due to the large heat load [1]. Extensive experimental results from recent years, on several existing tokamak devices [2, 3, 4, 5], have demonstrated that the externally applied resonant magnetic perturbation (RMP) fields can significantly affect the behavior of ELMs. It appears that the ELM mitigation/suppression, and the accompanying density pump-out effect observed in experiments, require detailed investigations due to complex physics.

One particularly important aspect is the RMP field penetration through the plasma. From the macroscopic point of view, this is a non-linear dynamic process involving at least two key effects. One is the plasma response to the applied external field. The plasma flow has been shown to play a critical role in screening the RMP field [6, 7, 8, 9, 10]. The other effect is the rotation braking, due to the plasma response to the external field. Both fluid (electromagnetic) and kinetic effects can induce torques damping the plasma flow, in the presence of external non-axisymmetric fields.

In this work, we present a fluid-based toroidal, quasi-linear model, describing the RMP penetration process on the macroscopic scale. The model couples the plasma response to a toroidal momentum balance equation, that includes source, sink and diffusion terms. The sink is provided by the fluid $\mathbf{j} \times \mathbf{b}$ torque and the neoclassical toroidal viscous (NTV) torque. A quasi-linear version (called MARS-Q) of the MARS-F code [11] is developed and tested. Modeling is carried out for a test toroidal equilibrium, with mid-plane RMP coils in the $n = 1$ configuration (n is the toroidal mode number).

Section 2 describes the quasi-linear model, the numerical implementation and the benchmark results. Section 3 reports the modeling results for the test toroidal equilibrium, where a parametric study is also carried out, in order to clarify the influence of certain physics parameters on the RMP penetration dynamics. Section 4 summarizes the results.

2 Toroidal RMP field penetration model

The model that we propose here couples the linear plasma response to the toroidal momentum balance of the plasma. Within the single n assumption, the plasma response remains essentially linear. The only non-linear terms come from the interaction between modes with the same n number, resulting in the $n = 0$ correction to the plasma equilibrium and to the toroidal flow speed. We neglect the plasma equilibrium correction [12], assuming that the amplitude of the applied RMP field is sufficiently small. The effect of the RMP field on the toroidal flow, however, can be significant due to momentum damping. The damped flow in turn changes the plasma response to the RMP field. This non-linear coupling is maintained in our model, which we shall call the quasi-linear RMP penetration model. In what follows, we describe both components of the model: the plasma response and the toroidal momentum balance.

2.1 Plasma response model

For the plasma response to the RMP fields, we consider a resistive, single fluid plasma model, with arbitrary toroidal flow and flow shear [10]. Detailed plasma response computations have been performed for both MAST and ITER plasmas [13] using this model.

$$\left(\frac{\partial}{\partial t} + in\Omega\right)\xi = \mathbf{v} + (\xi \cdot \nabla\Omega)R\hat{\phi}, \quad (1)$$

$$\begin{aligned} \rho\left(\frac{\partial}{\partial t} + in\Omega\right)\mathbf{v} &= -\nabla p + \mathbf{j} \times \mathbf{B} + \mathbf{J} \times \mathbf{b} - \rho [2\Omega\hat{\mathbf{Z}} \times \mathbf{v} + (\mathbf{v} \cdot \nabla\Omega)R\hat{\phi}] \\ &\quad - \rho\kappa_{\parallel} |k_{\parallel} v_{th,i}| [\mathbf{v} + (\xi \cdot \nabla)\mathbf{V}_0]_{\parallel}, \end{aligned} \quad (2)$$

$$\left(\frac{\partial}{\partial t} + in\Omega\right)\mathbf{b} = \nabla \times (\mathbf{v} \times \mathbf{B}) + (\mathbf{b} \cdot \nabla\Omega)R\hat{\phi} - \nabla \times (\eta\mathbf{j}), \quad (3)$$

$$\left(\frac{\partial}{\partial t} + in\Omega\right)p = -\mathbf{v} \cdot \nabla P - \Gamma P \nabla \cdot \mathbf{v}, \quad (4)$$

$$\mathbf{j} = \nabla \times \mathbf{b}, \quad (5)$$

where R is the plasma major radius, $\hat{\phi}$ the unit vector along the geometric toroidal angle ϕ of the torus, $\hat{\mathbf{Z}}$ the unit vector in the vertical direction in the poloidal plane. n is the toroidal harmonic number. The plasma resistivity is denoted by η . The variables $\mathbf{v}, \mathbf{b}, \mathbf{j}, p, \xi$ represent the perturbed velocity, magnetic field, current, pressure, and plasma displacement, respectively. The equilibrium plasma density, field, current, and pressure are denoted by $\rho, \mathbf{B}, \mathbf{J}, P$, respectively. $\Gamma = 5/3$ is the ratio of specific heats.

We assume that the plasma equilibrium flow \mathbf{V}_0 has the toroidal component only, $\mathbf{V}_0 = R\Omega\hat{\phi}$, with Ω being the angular frequency of the toroidal rotation. A parallel sound wave damping term is added to the momentum equation (2), with κ being a numerical coefficient determining the damping “strength”. $k_{\parallel} = (n - m/q)/R$ is the parallel wave number, with m being the poloidal harmonic number and q being the safety factor. $v_{th,i} = \sqrt{2T_i/M_i}$ is the thermal ion velocity, with T_i, M_i being the thermal ion temperature and mass, respectively. The parallel component of the perturbed velocity is taken along the equilibrium field line. The validity of this damping model, for the RMP field response computations, is discussed in Ref. [10].

For the purpose of the RMP response modeling, the vacuum field equations outside the plasma, the thin resistive wall equation (when applicable), and the coil equations (Ampere’s law) are solved together with the MHD equations for the plasma. The RMP field response modeling requires solving a linear antenna problem, where the source term is specified as the current flowing in the magnetic perturbation coils. Since this is a linear problem, for axi-symmetric equilibria, we only need to consider a single toroidal mode number n at one time. Therefore, the source current is assumed to have an $\exp(in\phi)$ dependence along the toroidal angle ϕ .

2.2 Toroidal momentum balance model

The toroidal momentum equation is derived from the force balance equation

$$\rho \frac{\partial \mathbf{V}}{\partial t} = \mathbf{J} \times \mathbf{B} - \nabla P - \nabla \cdot \boldsymbol{\pi} + \mathbf{S}. \quad (6)$$

where \mathbf{V} is the plasma flow velocity, $\boldsymbol{\pi}$ the viscous tensor, and \mathbf{S} denoting the source term for the force.

Following Ref. [14], the flux surface averaged toroidal moment $L = \rho \langle R^2 \rangle \Omega$ satisfies

$$\frac{\partial L}{\partial t} = D(L) + T_{NTV}(\omega_E) + T_{j \times b} + T_{\text{source}}, \quad (7)$$

where ω_E is the toroidal $E \times B$ drift frequency. The toroidal torque, due to the generalized viscous force $\nabla \cdot \boldsymbol{\pi}$, is split into three terms: the momentum diffusion and pinch term D , the toroidal component of the neoclassical toroidal viscosity (NTV) torque T_{NTV} and the fluid electromagnetic torque $T_{j \times b}$. The first term can be written as [15]

$$D = \frac{G}{s} \frac{\partial}{\partial s} \frac{s}{G} \left[\chi_M \langle |\nabla s|^2 \rangle \frac{\partial L}{\partial s} + V_{\text{pinch}} \langle |\nabla s| \rangle L \right], \quad G \equiv F \langle 1/R^2 \rangle,$$

where s labels the radial coordinate, F is the equilibrium poloidal current flux function, χ_M the (anomalous) toroidal momentum diffusion coefficient, and V_{pinch} the pinch velocity.

The torque T_{source} from Eq. (7) comes from the source force term \mathbf{S} in Eq. (6), denoting, for instance, the momentum input due to the neutral beam injection.

The surface averaged, toroidal electromagnetic $\mathbf{j} \times \mathbf{b}$ torque density is computed as

$$T_{j \times b} = \oint \mathbf{R} \mathbf{j} \times \mathbf{b} \cdot \hat{\phi} dS / \oint dS,$$

where R is the major radius, \mathbf{j} and \mathbf{b} are the (total) perturbed plasma current and magnetic field, respectively. S denotes the flux surface. It should be pointed out that the total toroidal torque, acting on the plasma column, can be either computed by integrating the torque density defined in the above equation across the whole plasma minor radius, or by direct evaluation of a surface integral, at an arbitrary surface in the vacuum region between the plasma boundary and the first conducting structure. The integrand of the surface integral is the product of the perturbed radial and toroidal field components only [16]. These two equivalent methods provide an internal check of the numerical implementation for the $\mathbf{j} \times \mathbf{b}$ torque density calculation. This internal check has been successfully performed in the MARS-Q code.

The NTV torque is computed here using formulas from Ref. [14], where various regimes (the so-called $v - \sqrt{v}$ and $1/v$ regimes, as well as the superbanana and superbanana plateau regimes) are smoothly connected. We point out that these formulas do not treat the exact pitch angle scattering operator, nor the particle resonance effects associated with the bounce frequency [18]. Despite this, the approximate formulas from Ref. [14] are reasonably well verified by numerical results [17]. Comparison of this NTV theory with experimental data in JET [19] and DIII-D [20] shows better than the order of magnitude agreement, as long as the plasma response is properly taken into account in computing the torque.

If we assume that a momentum balance has been achieved before applying the RMP field, with $(\Omega_0, L_0, \omega_E^0)$ satisfying

$$D(L_0) + T_{source} = 0.$$

After applying the RMP field (without changing other equilibrium conditions), we define

$$\Omega(t) = \Omega_0 + \Delta\Omega(t), \quad L(t) = L_0 + \Delta L(t), \quad \omega_E = \omega_E^0 + \Delta\omega_E = \omega_E^0 + \Delta\Omega,$$

and obtain the following momentum balance equation in the presence of RMPs

$$\frac{\partial \Delta L}{\partial t} = D(\Delta L) + T_{NTV}(\omega_E^0 + \Delta\Omega) + T_{j \times b}, \quad (8)$$

which is solved in MARS-Q, together with the linear MHD equations describing the plasma response to the RMP field. In the presence of the diffusion operator, equation (8) requires two boundary conditions, at the plasma center and edge, respectively. We use a Neumann type of boundary condition $\partial \Delta L / \partial s = 0$ at the plasma center. At the plasma edge, we assume a homogeneous Dirichlet boundary condition for ΔL . For tokamak plasmas, this is a reasonable approximation of the more generic Robin boundary condition, as demonstrated in Ref. [21], by considering a thin scrape-off layer surrounding the plasma.

It is now the proper time to discuss the validity of the above proposed quasi-linear model for the RMP field penetration computations. Obviously this is essentially a single fluid model, especially for the plasma response part. Inclusion of two fluid effects [22, 9, 23], as well as kinetic effects [7, 24] into the plasma response, remains our future work. In this work, we try to understand the MHD aspects of the RMP field penetration, by including the NTV torque into the momentum balance, and by considering a full toroidal geometry.

The other question is the validity of the model in terms of the time scale. Both experimental evidence and modeling results [24], including those to be shown in this work, seem to suggest

that the RMP penetration occurs at the time scale of several milliseconds, which is much slower than the Alfvénic time, but faster than the plasma resistive diffusion time. Therefore, at this time scale, we argue that the linear resistive response of the plasma, without inclusion of the finite island width effect, is appropriate. This is essentially the thin-island approximation, which is invalid for fully reconnected, large magnetic islands. Such islands form after the full penetration of the RMP field into the plasma.

On the other hand, we do not need to model the details of the Alfvén wave dynamics, which can be avoided by choosing a fully implicit time-stepping scheme for the full MHD equations. This time-stepping scheme is described in the following Subsection.

2.3 Time-stepping scheme for solving quasi-linear equations

The coupled MHD-momentum balance equations can be symbolically written as

$$\begin{aligned} B \frac{\partial X}{\partial t} &= A_1 X + Y A_2 X + X_0, \\ C \frac{\partial Y}{\partial t} &= D Y + T(Y) X^2, \end{aligned}$$

where the first equation is the full linearized MHD equation; with X denoting the full set of the existing MARS-F solution variables; $Y \equiv \Delta\Omega$ being the modification of the toroidal rotation frequency due to various torques, A_1 denoting the MHD operator, that also contains the initial rotation Ω_0 ; X_0 denoting the source term, i.e. the RMP current.

The second equation above is the momentum balance equation for Y . The first term from the right hand side denotes the linear momentum diffusion-pinch term. The second term from the right hand side denotes all the torque terms, with the coefficient T being generally a non-linear function of Y . The quadratic dependence of torques on the MHD perturbation variable X reflects the fact that the product of two $n \neq 0$ perturbations (the plasma current and the magnetic field) results in the $n = 0$ torque.

MARS-Q uses the following time stepping scheme based on a staggered grid in time

$$\begin{aligned} B \frac{X^{k+1} - X^k}{\Delta t} &= (1 - \alpha_2) A_1 X^k + \alpha_2 A_1 X^{k+1} + (1 - \alpha_3) Y^{k+1/2} A_2 X^k + \alpha_3 Y^{k+1/2} A_2 X^{k+1} + X_0, \\ C \frac{Y^{k+1/2} - Y^{k-1/2}}{\Delta t} &= (1 - \alpha_6) D Y^{k-1/2} + \alpha_6 D Y^{k+1/2} + T(Y^{k-1/2}) (X^{k+1})^2. \end{aligned}$$

where $\alpha_i, i = 1, \dots, 6$, are coefficients determining the numerical scheme of time stepping. We shall consider the RMP field penetration process (ms time scale) that is much faster than the Alfvén time $\tau_A \equiv R_0 \sqrt{\mu_0 \rho_0} / B_0$ (R_0, ρ_0, B_0 are the major radius, the plasma density, and the toroidal magnetic field at the plasma center, respectively), which is normally in the μs scale. This allows us to neglect the detailed dynamics of fast Alfvén waves, that can be achieved by choosing a fully implicit time-stepping scheme for the MHD operators, i.e. $\alpha_2 = \alpha_3 = 1$, and by choosing the time step Δt larger than 1. Our numerical computations for the test toroidal equilibrium show that Δt can be as large as $10\tau_A$, without compromising numerical accuracy

for the time trace, as will be shown later. Normally for time-stepping the momentum equation, we also choose the fully implicit scheme $\alpha_6 = 1$ for the linear operators.

We also designed a simple adaptive time-stepping scheme for solving the fully coupled equations, in which the time step depends on the iteration $\Delta t = \Delta t_k$. During the time-stepping, the code computes a quantity δ , characterizing the relative change of the solution (e.g. the $n \neq 0$ plasma response field and displacement) between two consecutive time steps. If δ is larger than a prescribed parameter δ_{\max} , the next time step is reduced by a factor $\alpha_7 < 1$, i.e. $\Delta t_{k+1} = \alpha_7 \Delta t_k$. If δ is smaller than a prescribed parameter δ_{\min} , the next time step is increased by the factor $1/\alpha_7$. For the modeling results shown in Sections 3, where the time adaptivity is applied, we choose $\delta_{\max} = 10\%$, $\delta_{\min} = 2\%$, and $\alpha_7 = 0.8$.

2.4 Benchmarking the momentum solver

The final momentum equation (8) is solved using a finite element method (FEM) along the radial grid. For simplicity, we assume homogeneous Neumann boundary conditions for ΔL at both the plasma center and edge in this analytic benchmark. [We note, though, that for physical problems to be solved in Section 3, we assume the Dirichlet boundary condition at the plasma edge.] With a given source term T which does not depend on time t and the solution y , Eq. (8) has a general form of

$$c \frac{\partial y}{\partial t} = \frac{1}{a} \frac{\partial}{\partial s} a \left(b \frac{\partial y}{\partial s} + dy \right) + T, \quad (9)$$

which allows an analytic steady state solution (which generally exists except some trivial cases)

$$\begin{aligned} y(s)|_{t \rightarrow \infty} &= \int_0^s \frac{e^{\alpha(t) - \alpha(s)}}{ab} \left[a_0 d_0 y_0 - \int_0^t a T du \right] dt + y_0 e^{-\alpha(s)}, \\ y_0 &= \left[a_1 d_1 a_0 d_0 \int_0^1 \frac{e^{\alpha(t) - \alpha(1)}}{ab} dt + a_1 d_1 e^{-\alpha(1)} - a_0 d_0 \right]^{-1} \times \\ &\quad \left[a_1 d_1 \int_0^1 \frac{e^{\alpha(t) - \alpha(1)}}{ab} dt \int_0^t a T du - \int_0^1 a T dt \right], \\ \alpha(s) &\equiv \int_0^s \frac{d}{b} dt, \end{aligned}$$

This analytic solution is used to test the FEM momentum solver in MARS-Q. A special case is considered, with

$$a(s) = a_0 e^{\beta s}, \quad b = b_0, \quad d = d_0, \quad \frac{d_0}{b_0} = \alpha, \quad T = T_0 e^{\gamma s},$$

and the steady state solution

$$y(s) = y_0 \frac{\alpha e^{-\beta s} - \beta e^{-\alpha s}}{\alpha - \beta} - \frac{T_0}{d_0} \frac{\alpha}{\beta + \gamma} \left(\frac{e^{\gamma s} - e^{-\alpha s}}{\alpha + \gamma} - \frac{e^{-\beta s} - e^{-\alpha s}}{\alpha - \beta} \right), \quad (10)$$

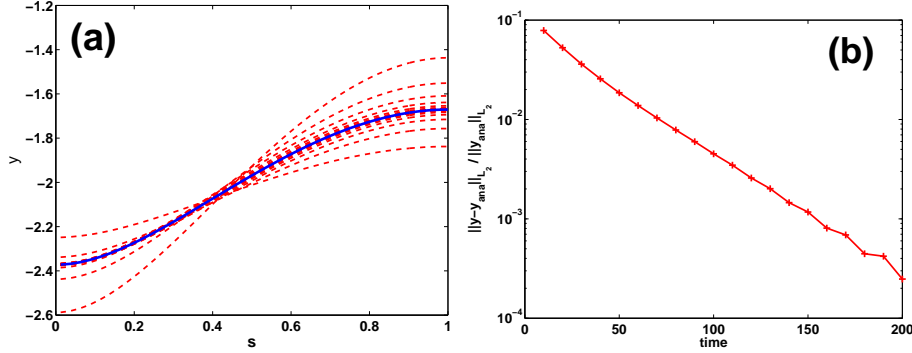


Figure 1: Test of the MARS-Q momentum solver against analytic solution (10), for a case with $a_0 = 2, d_0 = 3, T_0 = 3.2, \alpha = 1.5, \beta = 2.3, \gamma = 1.7$. Shown are (a) the convergence of the numerical profiles (dashed) to the analytic profile (solid), and (b) the convergence of the relative error of the solution, in L_2 norm, to the steady state analytic solution. The convergence of the radial profiles, shown in (a), comes from both sides of the dashed line, in an oscillating manner. The time step is chosen $\Delta t = 10$, with the implicitness parameter $\alpha_6=0.6$.

$$y_0 = \frac{T_0}{d_0} \frac{\alpha - \beta}{\beta(\beta + \gamma)} \left(\frac{\alpha}{\alpha + \gamma} - \frac{\alpha}{\alpha - \beta} + \frac{\gamma}{\alpha + \gamma} \frac{e^\gamma - e^{-\beta}}{e^{-\alpha} - e^{-\beta}} \right). \quad (11)$$

Figure 1 shows an example of the MARS-Q computed time evolution of Eq. (9), with the coefficient $c = 1$, the time step $\Delta t = 10$, and the implicitness parameter $\alpha_6=0.6$. The numerical solution converges to the analytic steady state solution. The convergence speed depends on the choice of parameter α_6 . At a given Δt , larger α_6 (i.e. more “implicit” scheme) usually gives faster convergence. Note that, since Eq. (9) represents a pure mathematical model, no specific physical units are associated with all the quantities here.

3 Numerical results for a test toroidal equilibrium

3.1 Equilibrium and RMP field configuration

The MARS-Q code allows quasi-linear simulations of the RMP field penetration dynamics and the plasma toroidal momentum damping, by coupling the $n \neq 0$ perturbed, full MHD equations with the $n = 0$ toroidal momentum balance equation. The modeling is performed for full toroidal geometry. The NTV torque is included into the momentum balance equation. Only toroidal plasma flow is considered. These are the major difference from a previous work [9], based on a four-field reduced MHD model, and cylindrical geometry.

We consider an analytic specification of the radial profiles for a toroidal equilibrium [10], in which the equilibrium current and pressure profiles, as well as the plasma boundary shape is specified analytically. The key radial profiles are shown in Fig. 2. The plasma major radius

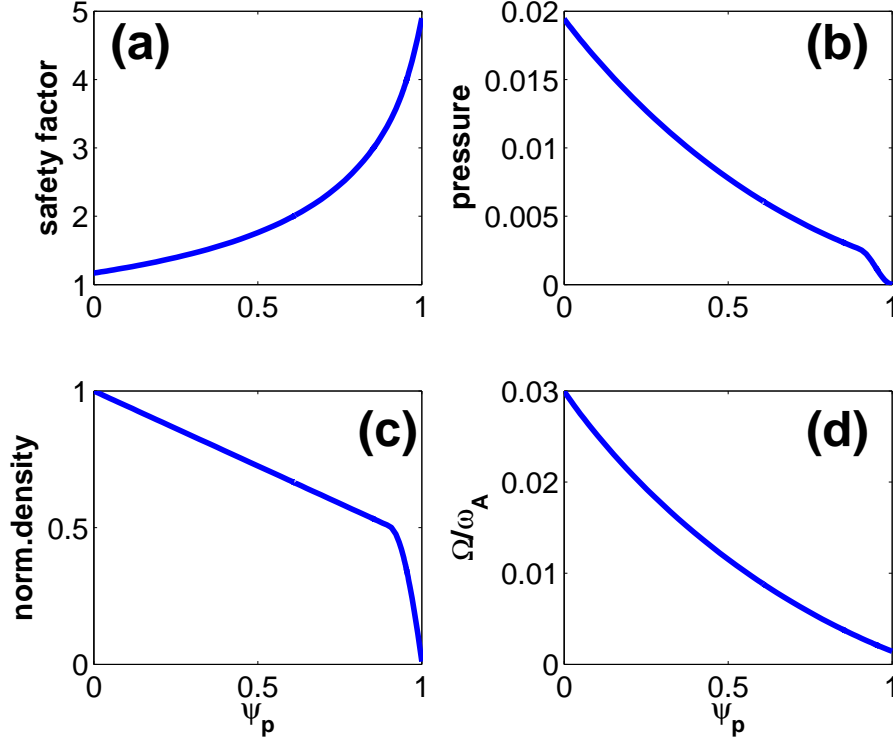


Figure 2: The radial profiles of the safety factor q , the equilibrium pressure (normalized by B_0^2/μ_0), the normalized plasma density (to unity at the magnetic axis), and the plasma toroidal rotation frequency Ω , for a test toroidal equilibrium.

of $R_0 = 3\text{m}$, the vacuum toroidal magnetic field $B_0=1.5\text{Tesla}$, and the aspect ratio $R_0/a = 3$. The plasma boundary has an elongation $\kappa = 1.6$ and triangularity $\delta = 0.3$. The equilibrium current and pressure are chosen to have $q_0 = 1.17, q_{95} = 3.94, q_a = 4.90$, and the normalized pressure $\beta_N = 1.56$. This plasma is far below the no-wall limit for the $n = 1$ ideal external kink instability. The total plasma current is 1.37MA .

For test computations, we consider the RMP field produced by a set of 4 coils located at $(R, Z) = (4.98, 1)\text{m}$ and $(4.98, -1)\text{m}$. These coils are uniformly distributed along the toroidal angle, each covering 90° toroidal angle. The coils are outside a resistive wall located at the minor radius of $1.23a$, resembling the error field correction coils (EFCC) in JET. The polarity of the coil currents are arranged to produce a predominantly $n = 1$ RMP field.

3.2 Numerical results for the base case

In order to investigate the effect of various physical and numerical parameters on the dynamics of the field penetration and the rotation damping, we first define a base case as follows. We consider a resistive plasma with the magnetic Lundquist number $S = 10^8$ at the magnetic axis. The radial profile of the plasma resistivity scales as $T_e^{-3/2}$, where T_e is the equilibrium thermal

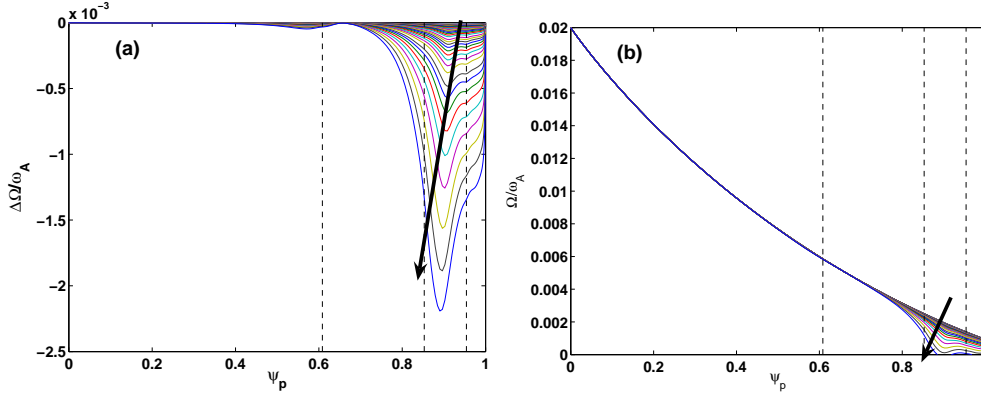


Figure 3: Evolution of the simulated radial profiles of (a) $\Delta\Omega(\psi_p, t) \equiv \Omega(\psi_p, t) - \Omega(\psi_p, t = 0)$ and (b) $\Omega(\psi_p, t)$ for the base case, where Ω is the toroidal rotation frequency, ψ_p is the normalized equilibrium poloidal flux, and t is the time. Shown are only profiles with a time span of 0.1ms, and after 10ms of simulation. The arrow indicates the time flow. The vertical dashed lines indicate radial locations of the $q = 2, 3, 4$ rational surfaces, respectively.

electron temperature. This leads to the S -value of about 10^6 near the plasma edge. We choose an amplitude of the anomalous toroidal momentum diffusion coefficient $\chi_M^0 = 3 \times 10^{-7} R_0 v_A \simeq 5 \text{ m}^2/\text{s}$, similar to the value in a typical JET plasma [25]. The radial profile of the momentum diffusion coefficient varies between two somewhat extreme examples. In the first example, which is used for the base case, $\chi_M(\psi_p) = \chi_M^0 \psi_p^{-2}$. This gives a larger momentum diffusion in the plasma core than in the edge. The other example, to be used later in this work, is $\chi_M(\psi_p) = \chi_M^0 [T_e(\psi_p)/T_e(0)]^{-3/2}$, which gives a larger momentum diffusion in the edge than in the core. The pinch velocity is neglected in this work. For the base case, both the $j \times b$ and NTV torques are included in the momentum equation. Finally, we assume that each of the RMP coils carries a 20kA current.

The direct consequence of the non-linear interaction between the plasma response (to the RMP fields) and the plasma flow is the flow damping, which is the primary effect that we report in this work. Figure 3 shows the evolution of the radial profile of the toroidal rotation frequency during this non-linear interaction, for the plasma and coil configurations as described for the base case. We obtain generally a full braking of the plasma flow near the edge region (beyond the $q = 3$ surface). A full penetration of the RMP field, into the plasma edge region, is expected as the rotation vanishes in that region. At full penetration, large magnetic islands form, which in turn invalidates the thin-island assumption used in the MARS-Q model. Therefore, generally speaking, our numerical results are valid only for the time interval before the full braking of the toroidal flow. We also note that, at the moment of the full rotation braking beyond the $q = 3$ surface, the core plasma rotation is still well maintained.

For this base case, as well as for other cases presented in this work, further time stepping does not yield a steady state solution. One possible reason is the violation of the quasi-linear assumption in the model, as discussed above. The other possibility is the development of (non-linear) MHD instabilities near the plasma edge region, where both the rotation and ro-

tation shear exhibit rapid changes. Allowing even further time evolution, the simulation produces numerically incorrect results. Therefore, for cases where no steady state solutions are reached, the physically meaningful solution is the time evolution before the full braking of the edge rotation of the plasma. This is also the physically interesting solution since it represents the dynamic process of the RMP field penetration. We mention that for certain plasmas, steady state solutions can be obtained by the MARS-Q quasi-linear model. Examples can be found from Ref. [20].

The observed rotation braking is caused by the electromagnetic and the NTV torques, whose radial profile evolution is shown in Fig. 4. Note that the $\mathbf{j} \times \mathbf{b}$ torque, though mainly occurring near rational surfaces, is nevertheless distributed along the minor radius, with non-trivial profiles. This is partially due to the continuum resonance induced splitting effect as discussed in [26]. The NTV torque, for the case considered here, is mainly localized between the $q = 3$ and 4 rational surfaces. This is in fact the major factor braking the plasma rotation between the $q = 3$ and 4 rational surfaces, as will be shown later (Fig. 9). However, we point out that this type of the NTV torque distribution, observed in most of the computations for the plasma studied in this work, should not be regarded as a ubiquitous feature valid for any plasma equilibria. The NTV torque is generally a rather non-linear function of the plasma $\mathbf{E} \times \mathbf{B}$ flow. In addition, the torque distribution also depends on the radial profile of the plasma collisionality, the drift kinetic resonance between the plasma response and plasma thermal particles, and finally on the spacial distribution of the perturbed 3D field amplitude $|\delta\mathbf{B}|$. All these factors can potentially affect the eventual radial profile of the NTV torque density. Figure 5 shows one example of the flux surface averaged $|\delta\mathbf{B}|$, normalized by the vacuum toroidal field at the magnetic axis, computed for the plasma response with the initial flow speed. The field amplitude predominantly comes from the Lagrangian variation (i.e. the field variation on the distorted flux surface). The computed field strength is of order of 10^{-3} of the vacuum field in the major part of the plasma column, but is larger near the plasma boundary, due to the larger plasma displacement towards the edge. More toroidal examples (and discussions of the above factors) are found in Ref. [20]. For the case considered here, we note that the amplitude of the NTV torque density is roughly about 5 times larger than that of the electromagnetic torque.

The time traces of the net (integrated over the plasma minor radius) electromagnetic and NTV torques are compared in Fig. 6, together with the time traces of the toroidal rotation frequencies at rational surfaces, for the base case. The net NTV torque is larger than the net $\mathbf{j} \times \mathbf{b}$ torque. But during the first ~ 10 ms of the time interval, the amplitudes of both torques are too small to cause appreciable damping of the flow (Fig. 6(b)). After about 10ms of simulation, the amplitudes of both torques rapidly increase, and the toroidal rotation quickly slows down in the region between the $q = 3$ rational surface and the plasma edge. The full time of the rotational damping (and hence the RMP penetration) is about 14ms for the base case.

3.3 Verification of time stepping scheme

For numerical efficiency, we wish to choose as large a time step as possible. Obviously, the time step cannot be chosen too large, in order not to affect the field penetration dynamics. A good criterion is that different choices of the time step should result in the same time evolution

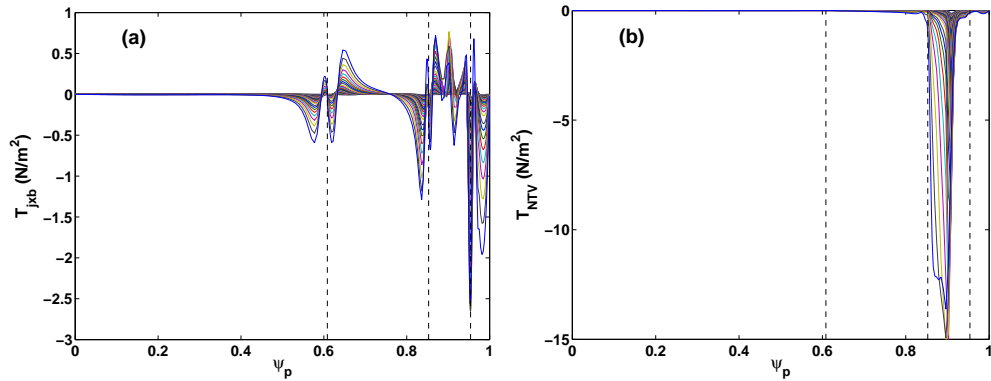


Figure 4: Evolution of the simulated radial profiles of (a) the electromagnetic torque density and (b) the NTV torque density for the base case. Shown are only profiles with a time span of 0.1ms, and after 10ms of simulation. The vertical dashed lines indicate radial locations of the $q = 2, 3, 4$ rational surfaces, respectively.

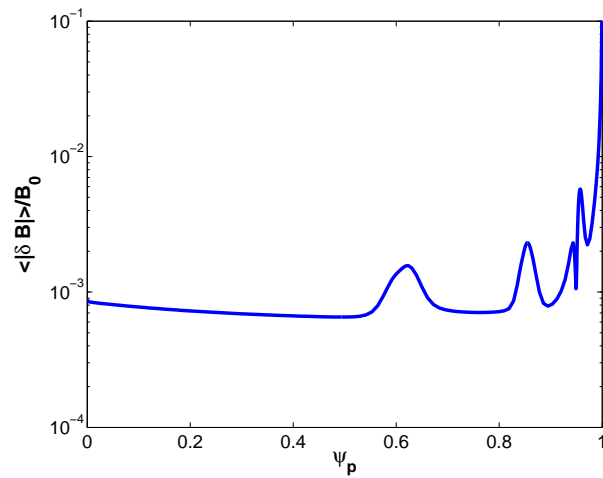


Figure 5: The radial profile of the flux surface averaged magnetic field strength including the plasma response, at the initial toroidal flow speed.

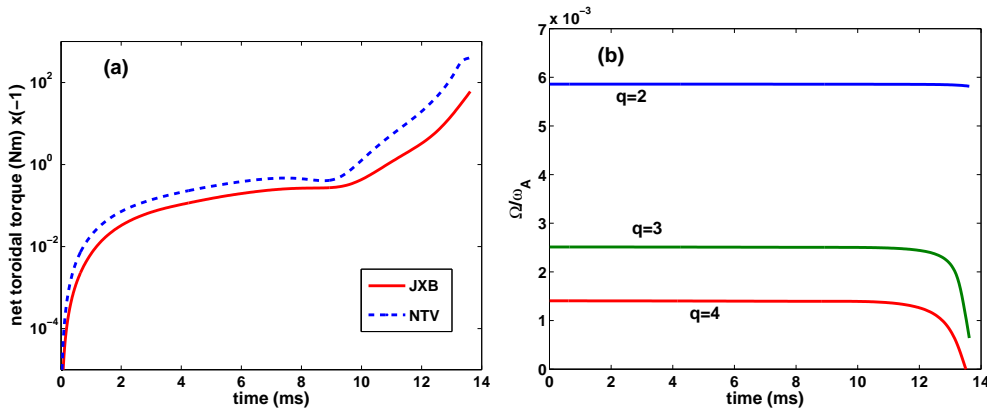


Figure 6: Simulated time traces of (a) the net toroidal electromagnetic and NTV torques (with reversed sign) acting on the plasma column, and (b) the toroidal rotation frequencies at the $q = 2, 3, 4$ rational surfaces, for the base case.

of the numerical solution. For the base case, we use an adaptive time stepping strategy as described in Section 2.3. The initial time step (at $t = 0$) is set to be $10\tau_A$. The time stepping history is shown in Fig. 7 as solid lines. For this case, the length of the time step steadily increases during the non-linear evolution. There are also cases where the length of the time step varies non-monotonically. For comparison, we run the same case, but with a fixed time step of $20\tau_A$ (dashed lines). The adaptive time stepping scheme requires much less number of steps to reach the same total simulation time. More importantly, the numerical solutions, as functions of time, agree well between two time stepping schemes, as shown in Fig. 8. This demonstrates the validity of our adaptive scheme.

3.4 Numerical results from parametric studies

Figure 6 shows that the NTV torque is generally the dominant momentum sink due to the interaction between the plasma response with the RMP field, for our plasma and coil configurations. It is therefore interesting to consider a case without inclusion of the NTV torque. The results are shown in Figs. 9 and 10, where only the electromagnetic torque is included in the toroidal momentum balance equation as the sink term. Compared to the base case, the only significant difference is that the flow velocity is much less damped between the $q = 3$ and 4 rational surfaces in the absence of the NTV torque. As a result, the full rotation braking (and hence the RMP penetration) occurs near the very edge of the plasma, mainly outside the $q = 4$ rational surface. In particular, the rotation velocity is still fully damped at the $q = 4$ surface, by the $\mathbf{j} \times \mathbf{b}$ torque alone. However, the full damping occurs slightly later (see Fig. 10(b)) than the base case, where both the electromagnetic and the NTV torques have been included into the momentum equation.

The plasma rotation braking, observed in this work, is not very sensitive to the radial profile of the toroidal momentum diffusion coefficient $\chi_M(\psi_p)$. In the simulation presented by Figs. 11

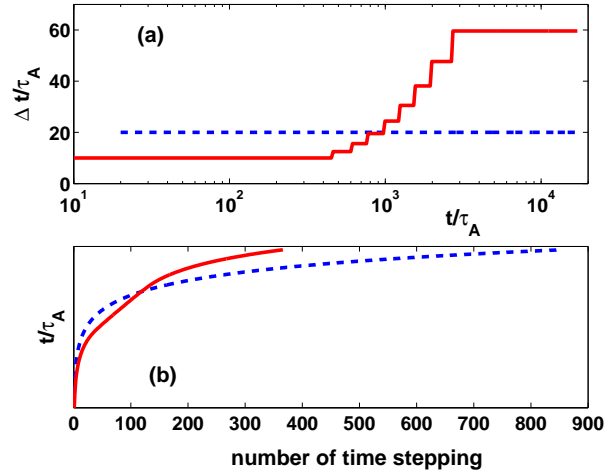


Figure 7: Comparison of the simulation history between the adaptive (solid lines) and fixed (dashed) time stepping schemes, for the base case: (a) the time step Δt versus the total simulation time t ; (b) the total simulation time t versus the number of time stepping.

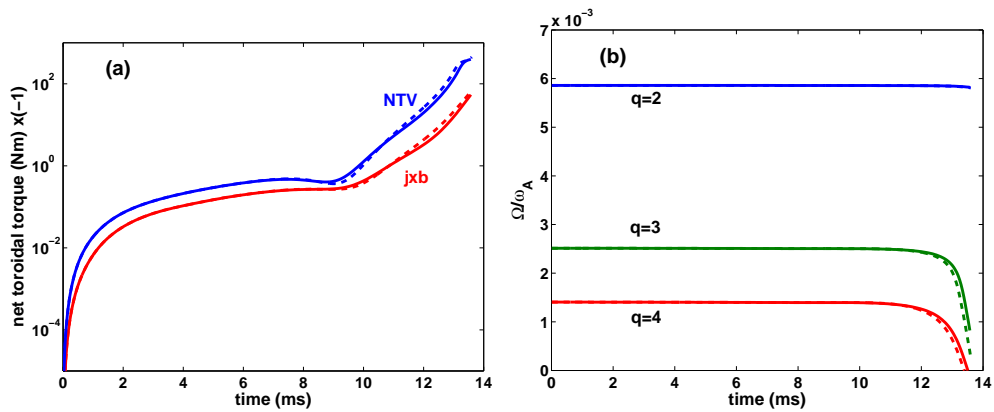


Figure 8: Simulated time traces of (a) the net toroidal electromagnetic and NTV torques (with reversed sign) acting on the plasma column, and (b) the toroidal rotation frequencies at the $q = 2, 3, 4$ rational surfaces, for the base case with adaptive (solid lines) and fixed (dashed lines) time stepping schemes.

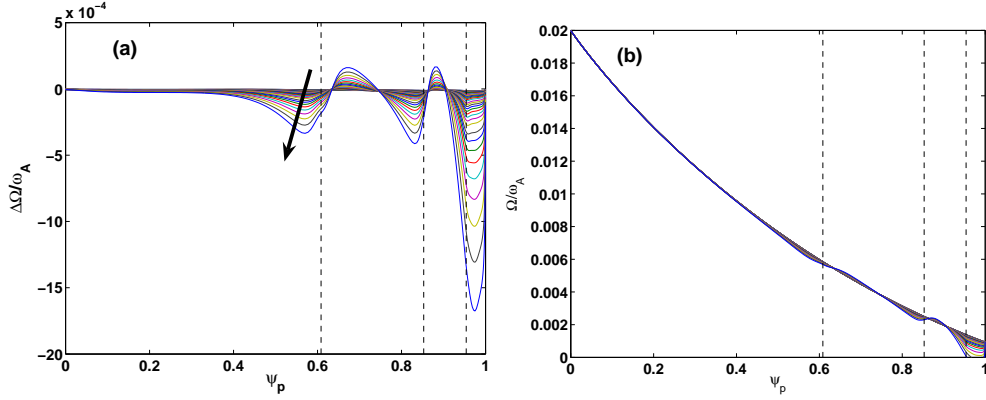


Figure 9: Evolution of the simulated radial profiles of (a) $\Delta\Omega(\psi_p, t) \equiv \Omega(\psi_p, t) - \Omega(\psi_p, t = 0)$ and (b) $\Omega(\psi_p, t)$ for the case without the NTV torque, where Ω is the toroidal rotation frequency, ψ_p is the normalized equilibrium poloidal flux, and t is the time. Shown are only profiles with a time span of 0.1ms, and after 10ms of simulation. The arrow indicates the time flow. The vertical dashed lines indicate radial locations of the $q = 2, 3, 4$ rational surfaces, respectively.

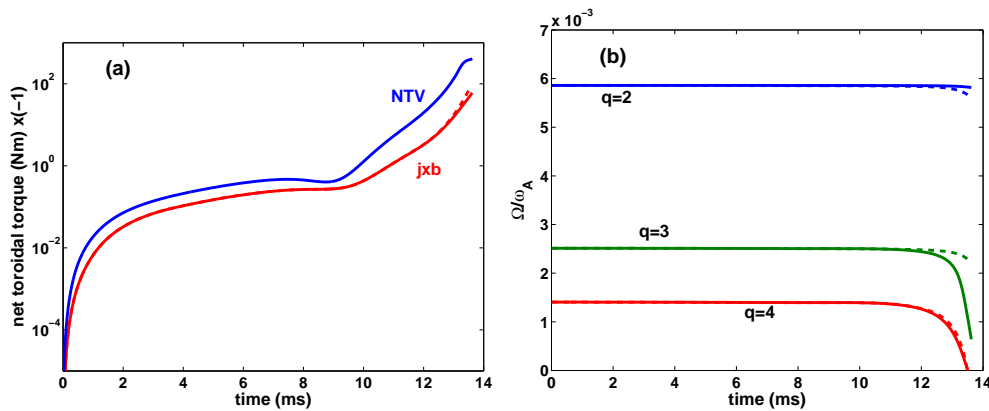


Figure 10: Simulated time traces of (a) the net toroidal electromagnetic and NTV torques (with reversed sign) acting on the plasma column, and (b) the toroidal rotation frequencies at the $q = 2, 3, 4$ rational surfaces, for the base case (solid lines) and the case without the NTV torque (dashed lines).

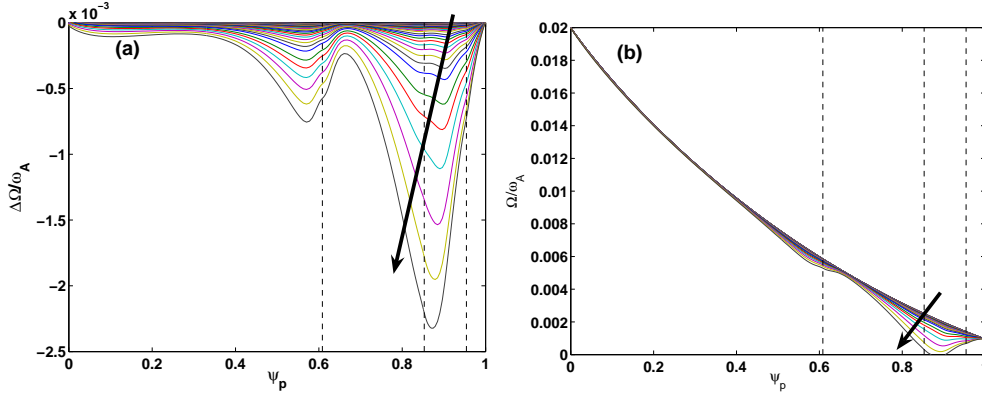


Figure 11: Evolution of the simulated radial profiles of (a) $\Delta\Omega(\psi_p, t) \equiv \Omega(\psi_p, t) - \Omega(\psi_p, t = 0)$ and (b) $\Omega(\psi_p, t)$ for the case with a radially increasing momentum diffusion, where Ω is the toroidal rotation frequency, ψ_p is the normalized equilibrium poloidal flux, and t is the time. Shown are only profiles with a time span of 0.1ms, and after 10ms of simulation. The arrow indicates the time flow. The vertical dashed lines indicate radial locations of the $q = 2, 3, 4$ rational surfaces, respectively.

and 12, we chose a completely different radial profile for χ_M , $\chi_M(\psi_p) = \chi_M^0 [T_e(\psi_p)/T_e(0)]^{-3/2}$, compared to the base case, yet the non-linear solutions do not significantly differ, apart from two observations. (i) Less flow damping is obtained near the plasma edge as shown in Fig. 11(b). This is because a large momentum diffusion near the plasma edge leads to a stronger coupling of the rotation velocity to the edge boundary condition, which is chosen to be fixed at a small but finite value. (ii) At all rational surfaces, the rotational braking occurs slower than the base case, as shown in Fig. 12. We note that the plasma core rotation is hardly affected by the RMP field, with both (extreme) types of the toroidal momentum diffusion profiles.

Finally, we also varied the amplitude of the RMP coil current. For this plasma equilibrium, it appears that even a small amount of the $n = 1$ RMP field can eventually brake the toroidal flow near the plasma edge. This may be due to the fact that a very low n field is applied to the plasma. Generally though, as expected, a lower current amplitude leads to weaker electromagnetic and NTV torques, and to a later braking of the rotation. One such example is shown in Figs. 13 and 14, where only half of the RMP current (i.e. 10kAt) is applied to the plasma, and the simulation results are compared with the 20kAt case (the base case).

4 Summary and discussion

A quasi-linear model is developed to study the RMP field penetration and the rotation braking in full toroidal geometry. The key physics, captured by this model, is the non-linear interplay between the damping of the plasma toroidal rotation by an external RMP field, and the screening of the RMP field due to the plasma rotation, as a result of the plasma response to the RMP field. Two toroidal torques - the electromagnetic $\mathbf{j} \times \mathbf{b}$ torque (fluid effect), and the NTV

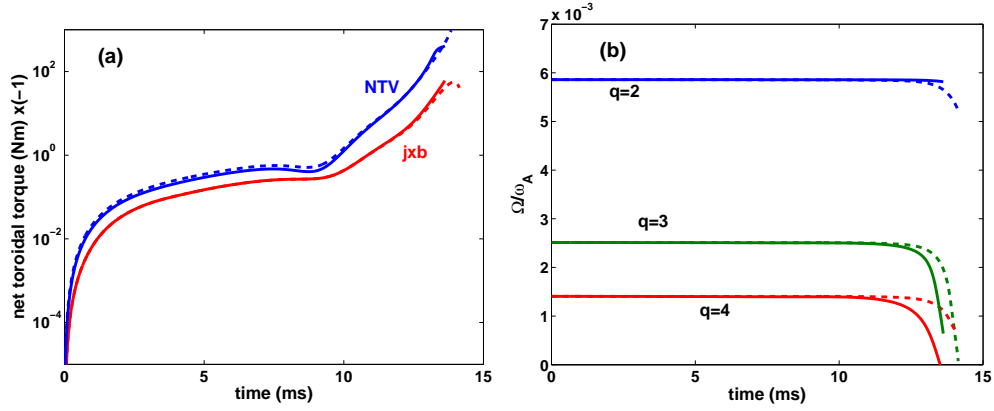


Figure 12: Simulated time traces of (a) the net toroidal electromagnetic and NTV torques (with reversed sign) acting on the plasma column, and (b) the toroidal rotation frequencies at the $q = 2, 3, 4$ rational surfaces, for the base case (solid lines) and the case with a radially increasing momentum diffusion (dashed lines).

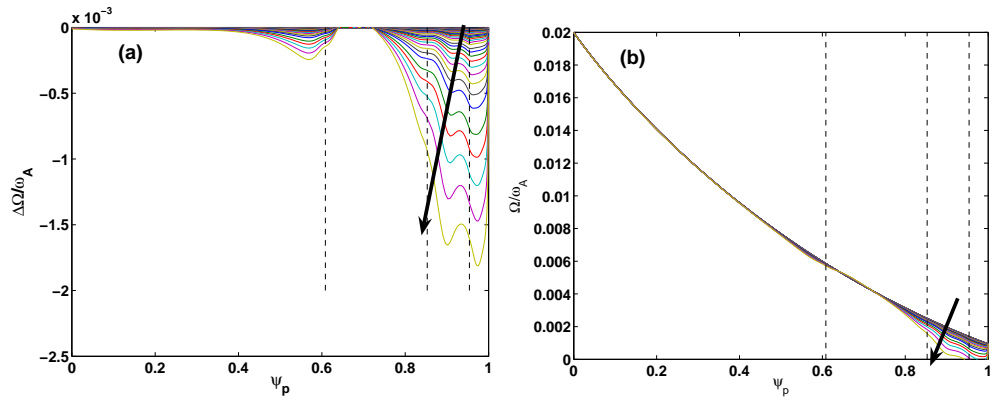


Figure 13: Evolution of the simulated radial profiles of (a) $\Delta\Omega(\psi_p, t) \equiv \Omega(\psi_p, t) - \Omega(\psi_p, t = 0)$ and (b) $\Omega(\psi_p, t)$ for the case with 10kAt coil current, where Ω is the toroidal rotation frequency, ψ_p is the normalized equilibrium poloidal flux, and t is the time. Shown are only profiles with a time span of 0.1ms, and after 10ms of simulation. The arrow indicates the time flow. The vertical dashed lines indicate radial locations of the $q = 2, 3, 4$ rational surfaces, respectively.

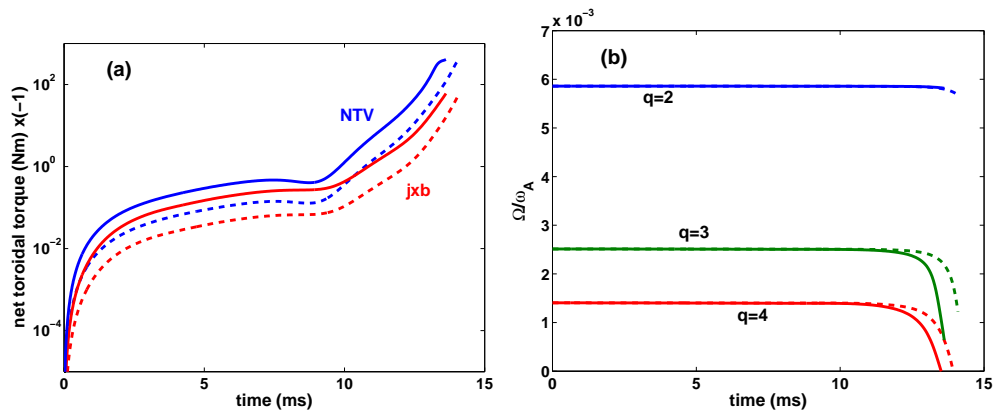


Figure 14: Simulated time traces of (a) the net toroidal electromagnetic and NTV torques (with reversed sign) acting on the plasma column, and (b) the toroidal rotation frequencies at the $q = 2, 3, 4$ rational surfaces, for the base case (20kAt, solid lines) and the case with half of the coil current (10kAt, dashed lines).

torque (kinetic effect) - are included in the toroidal momentum balance equation. An adaptive time stepping scheme is envisaged to speed up the non-linear simulations, which involves a fully implicit procedure for solving the MHD equations.

For a test toroidal equilibrium with H-mode plasma, we find that a $n = 1$ RMP field does not significantly change the plasma core rotation, *before* fully braking the rotation near the plasma edge region, most often outside the $q = 3$ rational surface. This observation does not exclude the core rotation damping in a longer time scale. However, our (thin island) model breaks down after the full damping the edge flow.

The toroidal computations quantify several factors affecting the dynamics of the RMP field penetration. (i) The plasma response to RMP fields induces a larger net NTV torque, than the $\mathbf{j} \times \mathbf{b}$ torque. This is not a ubiquitous observation, but does occur for the equilibrium considered in this work. Moreover, the NTV torque provides predominant flow damping between the $q = 3$ and 4 rational surfaces. (ii) Not surprisingly, we find that a larger RMP amplitude leads to stronger rotational damping and faster field penetration. The penetration time is generally in the order of ten milliseconds for our example. (iii) The radial profile of the momentum diffusion coefficient, which is an uncertain factor in our simulations, does not play a significant role for the flow damping observed in this study.

For the cases considered in this work, no steady state solution is found, although steady solutions are found by MARS-Q for other plasmas [20]. The boundary condition, assumed for the momentum balance equation at the plasma boundary, also affects the achievement of the steady state solution. For instance, by assuming a Neumann type of boundary condition, MARS-Q simulation can lead to steady state solutions. But these solutions are physically less relevant.

Even though the results presented in the paper mainly demonstrate the rotational braking ef-

fect due to the applied RMP field, it is worthwhile to further discuss some key aspects of the RMP field penetration itself, in particularly the penetration mechanism. In our model, the field penetration process is dictated by the strong non-linear interplay between the resistive plasma response and the toroidal flow damping. Therefore, the penetration time is eventually associated, from one side, with the resistive decay of the current sheets, formed near rational surfaces that tend to prevent the penetration of resonant field components, and from the other side, with the diffusion of the toroidal momentum. The scaling of the penetration time versus basic plasma and coil parameters, which has not been established in this initial work but will be systematically investigated in the future, is associated with these physics. For instance, we mention that a linear scaling of the penetration time, versus the magnetic Lundquist number, has been established in a cylindrical simulation [8]. No scaling has been established with respect to the plasma initial flow speed, though a qualitative understanding is possible relying on the following two arguments: (i) a slower initial flow (before applying the RMP field) normally yields less screening of the resonant field perturbations, and hence should facilitate the field penetration; (ii) at sufficiently slow rotation, the $\mathbf{E} \times \mathbf{B}$ flow frequency can be in resonance with the precessional drift frequency of trapped thermal particles, resulting in enhanced (resonant) NTV torque, which in turn can lead to a faster damping of the flow and hence the field penetration.

Another interesting question is whether the penetration time is associated with the Alfvén time, expected for establishing a magnetic equilibrium. It appears that both experimental evidence [20] and the numerical results shown in this work, as well as other theoretical work [8, 24], indicate that the resonant component of the applied magnetic field penetrates into the plasma in the milliseconds time scale, much slower than the Alfvén time.

We point out that the present study is based on a single fluid plasma model. It can be argued that the electron response may be important in the RMP field shielding. Therefore, a two-fluid model, or even a full kinetic model [24], may be necessary to better describe the plasma behavior in the presence of RMP fields. The possible field line stochastisation can induce an additional plasma radial current [27], and consequently field screening. These effects have not been taken into account in our present quasi-linear model.

Acknowledgments. YQL thanks Drs. I.T. Chapman, B.D. Dudson, G. Fishpool, R.J. Hastie, T.C. Hender, D.F. Howell, E. Nardon, V.D. Pustovitov, S. Saarelma, and A.J. Webster for very helpful discussions during this work, in particular Dr. Fishpool for suggesting the Dirichlet boundary condition for the momentum solver, and Dr. Chapman for many helpful suggestions improving the manuscript.

This work was part-funded by the RCUK Energy Programme under grant EP/I501045 and the European Communities under the contract of Association between EURATOM and CCFE. The views and opinions expressed herein do not necessarily reflect those of the European Commission.

Youwen Sun would like to acknowledge the support from the National Magnetic Confinement Fusion Science Program of China under Grant No. 2013GB102000 and No. 2012GB105000, and the National Natural Science Foundation of China under Grant No. 11205199 and No. 10725523.

We also thank the anonymous reviewer for interesting comments, that lead to discussions of the important issues associated with the field penetration mechanism.

References

- [1] A. Loarte, B. Lipschultz, A.S. Kukushkin, G.F. Matthews, P.C. Stangeby, N. Asakura, G.F. Counsell, G. Federici, A. Kallenbach, K. Krieger, A. Mahdavi, V. Philipps, D. Reiter, J. Roth, J. Strachan, D. Whyte, R. Doerner, T. Eich, W. Fundamenski, A. Herrmann, M. Fenstermacher, P. Ghendrih, M. Groth, A. Kirschner, S. Konoshima, B. LaBombard, P. Lang, A.W. Leonard, P. Monier-Garbet, R. Neu, H. Pacher, B. Pegourie, R.A. Pitts, S. Takamura, J. Terry, E. Tsitrone and the ITPA Scrape-off Layer and Divertor Physics Topical Group, *Nucl. Fusion* **47**, S203 (2007).
- [2] T.E. Evans, R.A. Moyer, K.H. Burrell, M.E. Fenstermacher, I. Joseph, A.W. Leonard, T.H. Osborne, G.D. Porter, M.J. Schaffer, P.B. Snyder, P.R. Thomas, J.G. Watkins, and W.P. West, *Nat. Phys.* **2**, 419 (2006).
- [3] Y. Liang, H.R. Koslowski, P.R. Thomas, E. Nardon, B. Alper, P. Andrew, Y. Andrew, G. Arnoux, Y. Baranov, M. Bcoulet, M. Beurskens, T. Biewer, M. Bigi, K. Crombe, E. De La Luna, P. de Vries, W. Fundamenski, S. Gerasimov, C. Giroud, M.P. Gryaznevich, N. Hawkes, S. Hotchin, D. Howell, S. Jachmich, V. Kiptily, L. Moreira, V. Parail, S.D. Pinches, E. Rachlew, and O. Zimmermann, *Phys. Rev. Lett.* **98**, 265004 (2007).
- [4] A. Kirk, E. Nardon, R. Akers, M. Bcoulet, G. De Temmerman, B. Dudson, B. Hnat, Y.Q. Liu, R. Martin, P. Tamain, D. Taylor and the MAST team, *Nucl. Fusion* **50**, 034008 (2010).
- [5] W. Suttrop, T. Eich, J. C. Fuchs, S. Guenter, A. Janzer, A. Herrmann, A. Kallenbach, P. T. Lang, T. Lunt, M. Maraschek, R. M. McDermott, A. Mlynek, T. Puetterich, M. Rott, T. Vierle, E. Wolfrum, Q. Yu, I. Zammuto, and H. Zohm (ASDEX Upgrade Team), *Phys. Rev. Lett.* **106**, 225004 (2011).
- [6] F.L. Waelbroeck, *Phys. Plasmas* **10**, 4040 (2003).
- [7] M.F. Heyn, I.B. Ivanov, S.V. Kasilov, W. Kernbichler, I. Joseph, R.A. Moyer and A.M. Runov, *Nucl. Fusion* **48**, 024005 (2008).
- [8] M. Bécoulet, G. Huysmans, X. Garbet, E. Nardon, D. Howell, A. Garofalo, M. Schaffer, T. Evans, K. Shaing, A. Cole, J.-K. Park and P. Cahyna, *Nucl. Fusion* **49**, 085011 (2009).
- [9] E. Nardon, P. Tamain, M. Bécoulet, G. Huysmans and F.L. Waelbroeck, *Nucl. Fusion* **50**, 034002 (2010).
- [10] Y.Q. Liu, A. Kirk and E. Nardon, *Phys. Plasmas* **17**, 122502 (2010).
- [11] Y.Q. Liu, A. Bondeson, C.M. Fransson, B. Lennartson and C. Breitholtz, *Phys. Plasmas* **7**, 3681 (2000).

- [12] I.T. Chapman, T.C. Hender, D.F. Howell, S.K. Erents, M. P. Gryaznevich, S. Shibaev, M.F. Stamp, E. de la Luna, A. Savchkov, R. Scannell, the MAST team and JET EFDA Contributors, *Nucl. Fusion* **47**, L36 (2007).
- [13] Y.Q. Liu, A. Kirk, Y. Gribov, M.P. Gryaznevich, T.C. Hender and E. Nardon, *Nucl. Fusion* **51**, 083002 (2011).
- [14] K.C. Shaing, S.A. Sabbagh and M.S. Chu, *Nucl. Fusion* **50**, 025022 (2010).
- [15] Y. Sun, Y. Liang, H.R. Koslowski, S. Jachmich, A. Alfier, O. Asunta, G. Corrigan, C. Giroud, M.P. Gryaznevich, D. Harting, T. Hender, E. Nardon, V. Naulin, V. Parail, T. Tala, C. Wiegmann, S. Wiesen and JET-EFDA contributors, *Plasma Phys. Control. Fusion* **52**, 105007 (2010).
- [16] V.D. Pustovitov, *Nucl. Fusion* **47**, 1583 (2007).
- [17] Y. Sun, Y. Liang, K.C. Shaing, H.R. Koslowski, C. Wiegmann, and T. Zhang, *Phys. Rev. Lett.* **105**, 145002 (2010).
- [18] J.-K. Park, A.H. Boozer, and J.E. Menard, *Phys. Rev. Lett.* **102**, 065002 (2009).
- [19] Y. Sun, Y. Liang, K.C. Shaing, Y.Q. Liu, H.R. Koslowski, S. Jachmich, A. Alfier, O. Asunta, P. Buratti, G. Corrigan, E. Delabie, C. Giroud, M.P. Gryaznevich, D. Harting, T. Hender, E. Nardon, V. Naulin, V. Parail, T. Tala, C. Wiegmann, S. Wiesen, T. Zhang and JET-EFDA contributors, *Nucl. Fusion* **52**, 083007 (2012).
- [20] Y.Q. Liu, A. Kirk, Y.Sun, P. Cahyna, I.T. Chapman, P. Denner, G. Fishpool, A.M. Garofalo, J.R. Harrison, E. Nardon, and the MAST team, *Plasma Phys. Control. Fusion* **54**, 124013 (2012).
- [21] R. Fitzpatrick, *Nucl. Fusion* **33**, 1049 (1993).
- [22] Q. Yu, S. Guenter and K.H. Finken, *Phys. Plasmas* **16**, 042301 (2009).
- [23] N.M. Ferraro, *Phys. Plasmas* **19**, 056105 (2012).
- [24] G Park, C. S. Chang, I. Joseph, and R. A. Moyer, *Phys. Plasmas* **17** 102503 (2010).
- [25] Yu.F. Baranov, I. Jenkins, B. Alper, C.D. Challis, S. Conroy, V. Kiptily, J. Ongena, S. Popovichev, P. Smeulders, E. Surrey, K.-D. Zastrow and JET EFDA contributors, *Plasma Phys. Control. Fusion* **51**, 044004 (2009).
- [26] Y.Q. Liu, J.W. Connor, S.C. Cowley, C.J. Ham, R.J. Hastie, and T.C. Hender, *Phys. Plasmas* **19**, 102507 (2012).
- [27] V. Rozhansky, E. Kaveeva, P. Molchanov, I. Veselova, S. Voskoboynikov, D. Coster, A. Kirk, S. Lisgo and E. Nardon, *Nucl. Fusion* **50**, 034005 (2010).